Heliyon 9 (2023) e18478

Contents lists available at ScienceDirect

Heliyon

journal homepage: www.cell.com/heliyon

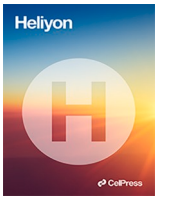

Unsteady mhd flow of tangent hyperbolic liquid past a vertical porous plate plate

Naga Pavani M [a], G. Venkata Ramana Reddy [b], Ali Akgül [c,d,e], Muhammad Bilal Riaz [f,g,h,*]

[a] Research Scholar, Department of Engineering Mathematics, Koneru Lakshmaiah Education Foundation, Vaddeswaram, 522302, India
[b] Department of Engineering Mathematics, Koneru Lakshmaiah Education Foundation, Vaddeswaram, 522302, India
[c] Department of Computer Science and Mathematics, Lebanese American University, Beirut, Lebanon
[d] Siirt University, Art and Science Faculty, Department of Mathematics, 56100 Siirt, Turkey
[e] Near East University, Mathematics Research Center, Department of Mathematics, Near East Boulevard, PC: 99138, Nicosia /Mersin 10, Turkey
[f] Faculty of Technical Physics, Information Technology and Applied Mathematics, Lodz University of Technology, 90-924 Lodz, Poland
[g] Department of Computer Science and Mathematics, Lebanese American University, Byblos, Lebanon
[h] Department of Mathematics, University of Management and Technology, 54770 Lahore, Pakistan

ARTICLE INFO

Keywords:
Joule heating
Non-Newtonian liquid
Spectral relaxation method

ABSTRACT

The analysis in this communication addresses the unsteady MHD flow of tangent hyperbolic liquid through a vertical plate. The model on mass and heat transport is set up with Joule heating, heat generation, viscous dissipation, thermal radiation, chemical reaction and Soret-Dufour in the form of partial differential equations (PDEs). The PDEs are simplified into a dimensionless PDEs by utilizing a suitable quantities. The simplified equations are solved by utilizing the spectral relaxation method (SRM). The outcomes shows that increase in the Weissenberg and the magnetic field degenerates the velocity profile. The thermal radiation is found to elevate the velocity and temperature profiles as its values increases. The impact of Soret and Dufour on the flow is found to alternate each other. The computational outcomes for concentration, temperature and velocity are illustrated graphically for all encountered flow parameters. The present outcomes are compared with previous outcomes and are found to correlate.

1. Introduction

The study of non-Newtonian liquid is more comprehensive when compared with Newtonian liquid. The non-Newtonian liquids possesses variable viscosity owning to the presence of an applied force. In analysing non-Newtonian liquid behaviour, many constitutive model equations have been utilized in literature. The tangent hyperbolic liquid is good enough to describe the phenomenon of shear thinning. Fluids of this type are blood, paint, ketchup etc. Different physical properties are described in literature to explain tangent hyperbolic fluid [1]. elucidate MHD tangent hyperbolic liquid past a nonlinear and stretchable sheet viscous dissipation as well as convective boundary constraints [2]. elucidate Soret and radiation effects on an unsteady flow of a casson fluid through porous vertical channel with expansion and contraction. [3] elucidate Soret and dufour effects on MHD micropolar fluid flow over a linearly

* Corresponding author. Faculty of Technical Physics, Information Technology and Applied Mathematics, Lodz University of Technology, 90-924 Lodz, Poland.
E-mail address: bilalsehole@gmail.com (M. Bilal Riaz).

https://doi.org/10.1016/j.heliyon.2023.e18478
Received 17 May 2022; Received in revised form 18 July 2023; Accepted 19 July 2023
Available online 2 August 2023

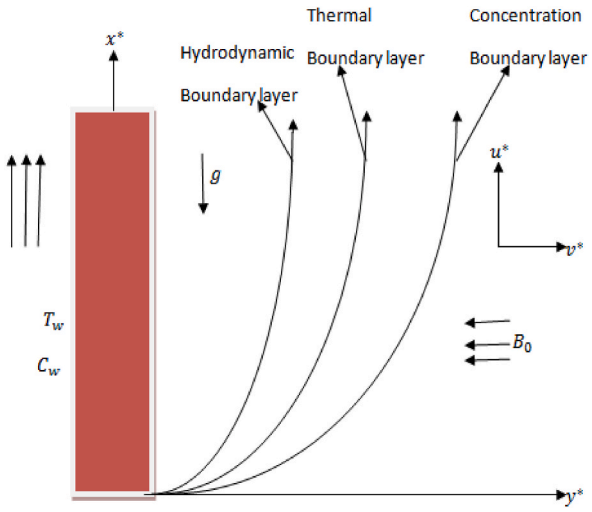

Fig. 1. Physical geometry.

stretching sheet, through a non-darcy porous medium. [4] presents A study on free convective heat and mass transfer flow through a highly porous medium with radiation, chemical reaction and soret effects [5]. elucidate Non-linear density variation in micro polar fluid on a convectively heated elongated surface with second order slip [6]. inspected the MHD flow of tangent hyperbolic liquid with nanoparticles and convective boundary constraints [7]. utilizes spectral relaxation techniques to solve the problem of MHD boundary layer flow of tangent hyperbolic liquid past a stretchable cylinder [8]. explored the flow of hyperbolic tangent liquid past a slanting exponentially stretchable cylinder. Zakir and Gul [9] did analysis of Lie group on hyperbolic tangent liquid with MHD and slip constraints [10]. elucidate the nano liquid flow of dusty hyperbolic in two phase. The peristaltic flow of hyperbolic tangent liquid in three dimensional and non-uniform medium have been elucidated by Ref. [11].

The MHD flow of non-Newtonian liquids have gained attention in recent time owning to its important in physics and engineering. In the problem of heat alongside mass transport, the MHD nature of an electrically conducting liquid produces the Lorentz force. This force explain the usefulness of the imposed magnetism in controlling turbulence flow. However, the MHD finds applications in nuclear power plants, MHD accelerators, gas turbines, geophysics etc. [12] explored the MHD flow of a chemically reacting liquid by utilizing spectral relaxation technique [13]. discussed MHD flow of Casson liquid past a slanting penetrable stretchable surface [14]. presented the impact of varying Lorentz force on nanoliquid flow using analytical approach [15]. gives detailed analysis on unsteady MHD Eyring-Powell flow in stretchable medium. The flow of Powell-Eyring MHD nano materials have been elucidated by Ref. [16]. [17] inspected MHD thin film on radiative Williamson liquid past a penetrable stretching sheet. The recent study of [18] explained the behaviour of MHD while varying viscosity alongside thermal conductivity [2]. discussed the unsteady flow of MHD Casson liquid with thermal radiation [3]. discussed MHD micropolar liquid flow with Soret-Dufour influence [4]. studied heat and mass transport flow with MHD and thermal radiation.

The thermal radiation and chemical reaction plays a significant role in engineering and applied science. Its industrial applications are found in furnace design, and glass production, plasma physics, propulsion system etc. [19] discussed the impact of thermal radiation alongside nanoparticles on heat transport of Casson liquid [20]. recently examined thermal radiation alongside chemically reacting MHD fluids in porous channel [21]. studied heat transport of dusty hyperbolic tangent liquid with thermal radiation as well as magnetic field [22]. discussed thermal radiation alongside heat sources on MHD flow of viscoelastic liquid. The recent study of [23] elucidate unsteady problem of MHD convective flow with thermal radiation and thermophoresis influence [24]. used spectral relaxation technique to explain the behaviour of Walters-B liquid with thermal radiation and Soret-Dufour influence. Y. Damodhar Reddy et al. [25] elucidate Radiation, velocity and thermal slips effect towards MHD boundary layer flow Through Heat and Mass Transport of Williamson Nano fluid with Porous Medium. Souad Marzougui et al. [26] elucidate Entropy generation and heat transport of Cu–water nanoliquid in porous lid-driven cavity through magnetic field.

Motivated by the above literature reviewed, this communication is concentrated on the effects of Lorentz force, Joule heating and viscous dissipation on unsteady flow of tangent hyperbolic liquid past a vertical plate. Study of this type has not been considered in literature to the best of our knowledge. Hence, we communicate this analysis owning to the practical applications in science and engineering such as the use of Lorentz force in MHD accelerators, chemical catalytic reactors, Soret in isotope separation etc. The flow PDEs are solved numerically using SRM and effects of encountered parameters are presented in graphs.

1.1. Flow analysis

Consider laminar, unsteady, two-dimensional flow of MHD tangent hyperbolic liquid past a semi-infinite vertical penetrable plate with viscous dissipation and thermal radiation. The plate is presumed to be infinite in x^*-direction while y^*-direction is normal to it (see

Fig. 1). The movement of the upward plate is presumed only towards the y^*-axis, hence the derivative $\frac{\partial u^*}{\partial x^*}$ is forgone. Initially when the fluid is set into motion, the time $t^* \leq 0$ both the plate alongside the fluid maintains uniform temperature. In view of this, thermal radiation along with heat generation is taking into account. A magnetism of uniform strength (B_0) is transversely imposed to both plate and flow direction. The magnetic Reynolds number is assumed to be small such that induced magnetic field is forgone. The level of species is assumed to be high such that Soret-Dufour effects are considered. Following [1] and the definition of Cauchy stress tensor T as:

$$T = -pI + S \tag{1}$$

The constitutive analysis of extra tensor S of tangent hyperbolic liquid as described by Ref. [1] gives

$$S = [\mu_\infty + (\mu_0 + \mu_\infty)\tanh\,(\Gamma\dot{\gamma})^n]A_1 \tag{2}$$

where μ_∞ signifies shear rate viscosity, μ_0 signifies zero shear rate viscosity, Γ signifies dependent material constant, n signifies the power law index, A_1 signifies the first tensor Rivlin-Erickson. From the above, $\dot{\gamma}$ gives:

$$\dot{\gamma} = \sqrt{\frac{1}{2}tr(A_1^2)} \tag{3}$$

For the sake of simplicity, consider $\mu_\infty = 0$ in equation (2) and since tangent hyperbolic liquid explains shear thinning analysis. Therefore, $\Gamma \det \gamma < 1$. Utilizing the above simplifications on equation (2) to obtain:

$$S = \mu_0[(\Gamma\dot{\gamma})]A_1 \tag{4}$$

Simplifying the above to obtain

$$S = \mu_0[1 + n(\Gamma\dot{\gamma} - 1)]A_1 \tag{5}$$

Under the assumptions above, the flow equations along with the boundary constraints are:

$$\frac{\partial v^*}{\partial y^*} = 0 \tag{6}$$

$$\frac{\partial u^*}{\partial t^*} + v^*\frac{\partial u^*}{\partial y^*} = \nu(1-n)\frac{\partial^2 u^*}{\partial y^{*2}} + \sqrt{2}\nu n\Gamma\frac{\partial u^*}{\partial y^*}\frac{\partial^2 u^*}{\partial y^{*2}} - \frac{\sigma B_0^2}{\rho}u^* + g\beta_t(T - T_\infty) + g\beta_c(C - C_\infty) \tag{7}$$

$$\frac{\partial T}{\partial t^*} + v^*\frac{\partial T}{\partial y^*} = \alpha\frac{\partial^2 T}{\partial y^*} + \frac{\nu}{c_p}\left(\frac{\partial u^*}{\partial y^*}\right)^2 - \frac{1}{\rho c_p}\frac{\partial q_r}{\partial y^*} + \frac{Q_0}{rhoc_p}(T - T_\infty) + \frac{Dk_T}{c_s c_p}\frac{\partial^2 C}{\partial y^{*2}} + \frac{\sigma B_0^2}{\rho c_p}u^2 \tag{8}$$

$$\frac{\partial C}{\partial t^*} + v^*\frac{\partial C}{\partial y^*} = D\frac{\partial^2 C}{\partial y^{*2}} + \frac{Dk_T}{T_m}\frac{\partial^2 T}{\partial y^{*2}} - K_r(C - C_\infty) \tag{9}$$

subject to the constraints:

$$u = U_0, T = T_w + \psi(T_w - T_\infty)e^{n^* t^*}, C = C_w + \psi(C_w - C_\infty)e^{n^* t^*}, at\ \ y^* = 0 \tag{10}$$

$$u^* \to 0, T \to T_\infty, C \to C_\infty, as\ \ y^* \to \infty \tag{11}$$

We obtain the suction velocity normal to the plate by integrating both sides of equation (1). Following the analysis presented by Ref. [24]; the wall suction velocity is a function of constant and time-dependent given as

$$v^* = -v_0\left(1 + \varepsilon A e^{n^* t^*}\right) \tag{12}$$

In this analysis, the radiative heat flux is assumed to be $\frac{\partial q_r}{\partial y^*} \gg \frac{\partial q_r}{\partial x^*}$ since the heat flux diverges only towards y^*-direction. Hence, the heat flux $\frac{\partial q_r}{\partial y^*}$ dominates the fluid flow. Considering that the difference in temperature throughout the flow is small in a way that T^4 is evaluated as a linear function of the ambient temperature T_∞. Simplifying T^4 in Taylor's approach in T_∞ and forgone terms of higher order to obtain:

$$T^4 \approx 4T_\infty^3 T - 3T_\infty^4 \tag{13}$$

Utilizing Rosse; and approximation, the heat flux in terms of y^* gives

$$q_r = -\frac{4\sigma_0}{3ke}\frac{\partial T^4}{\partial y^*} \tag{14}$$

here σ_0 signifies Stefan-Boltzmann constant and ke signifies mean absorption coefficient. Since the Rosseland approximation is utilized in this analysis, the tangent hyperbolic liquid is assumed to be optically thick liquids. Linearizing the (9) above and utilizing the

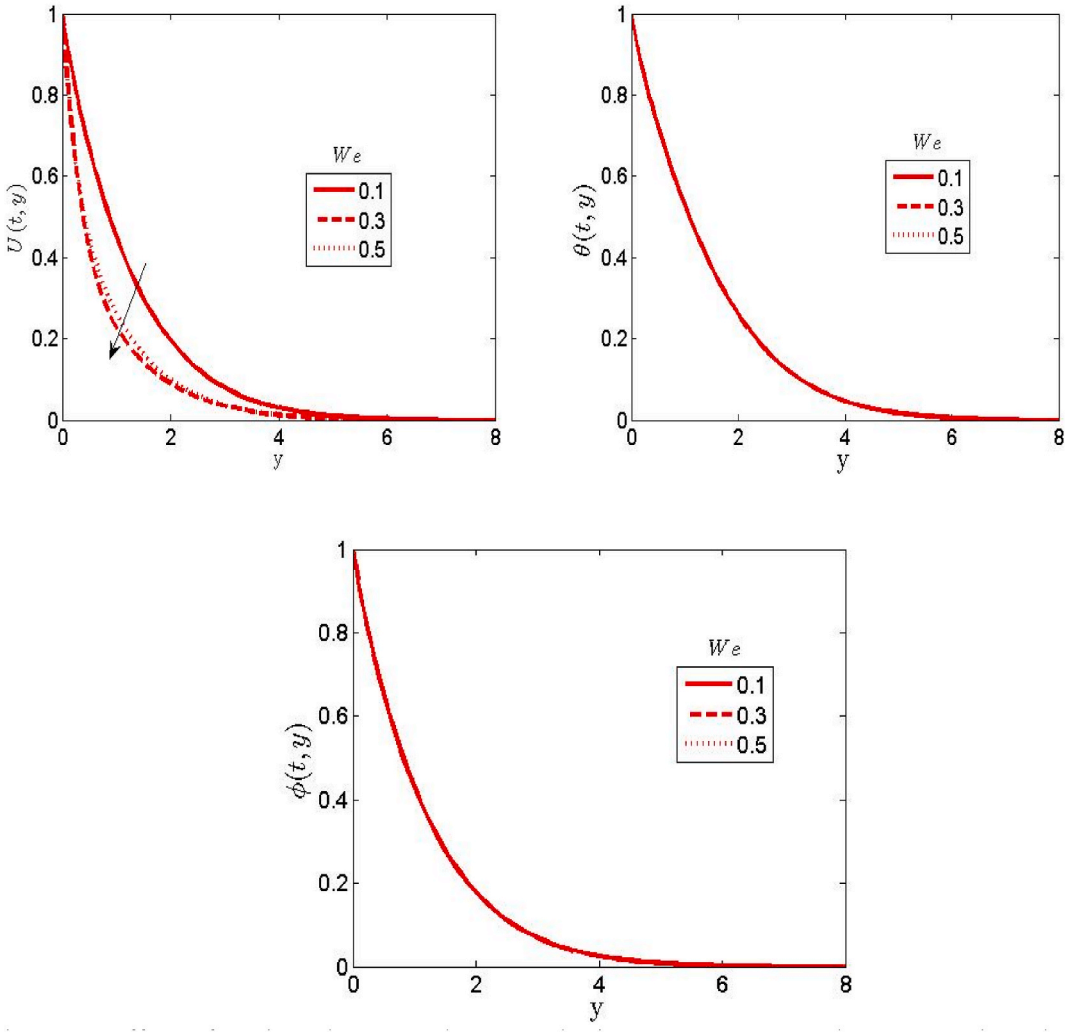

Fig. 2. Effect of Weissenberg number on velocity, temperature and concentration plots.

outcome on the energy equation to obtain

$$\frac{\partial T}{\partial t^*}+v^*\frac{\partial T}{\partial y^*}=\alpha\frac{\partial^2 T}{\partial y^*}+\frac{\nu}{c_p}\left(\frac{\partial u^*}{\partial y^*}\right)^2+\frac{16\sigma_0}{3\rho c_p ke}T_\infty^3\frac{\partial^2 T}{\partial y^{*2}}+\frac{Q_0}{rhoc_p}(T-T_\infty)+\frac{Dk_T}{c_s c_p}\frac{\partial^2 C}{\partial y^{*2}}+\frac{\sigma B_0^2}{\rho c_p}u^2 \tag{15}$$

To simplify the flow equations in a dimensionless form, the following quantities are introduced

$$u=\frac{u^*}{u_0}, y=\frac{v_0^2 y^*}{\nu}, t=\frac{v_0^2 t^*}{\nu}, n=\frac{\nu n^*}{v_0^2}, \theta=\frac{T-T_\infty}{T_w-T_\infty}, \varphi=\frac{C-C_\infty}{C_w-C_\infty} \tag{16}$$

Utilizing the above quantities on the flow equations with the boundary constraints to obtain the following flow PDEs:

$$\frac{\partial u}{\partial t}-(1+\varepsilon Ae^{nt})\frac{\partial u}{\partial y}=(1-n)\frac{\partial^2 u}{\partial y^2}+nWe\frac{\partial u}{\partial y}\frac{\partial^2 u}{\partial y^2}-M^2u+Gr\theta+Gm\varphi \tag{17}$$

$$\frac{\partial \theta}{\partial t}-(1+\varepsilon Ae^{nt})\frac{\partial \theta}{\partial y}=\left(\frac{1+R}{Pr}\right)\frac{\partial^2 \theta}{\partial y^2}+Ec\left(\frac{\partial u}{\partial y}\right)^2+Du\frac{\partial^2 \varphi}{\partial y^2}+\delta_x\theta+M^2Ecu^2 \tag{18}$$

$$\frac{\partial \varphi}{\partial t}-(1+\varepsilon Ae^{nt})\frac{\partial \varphi}{\partial y}=\left(\frac{1}{Sc}\right)\frac{\partial^2 \varphi}{\partial y^2}-Kr\varphi+So\frac{\partial^2 \theta}{\partial y^2} \tag{19}$$

subject to:

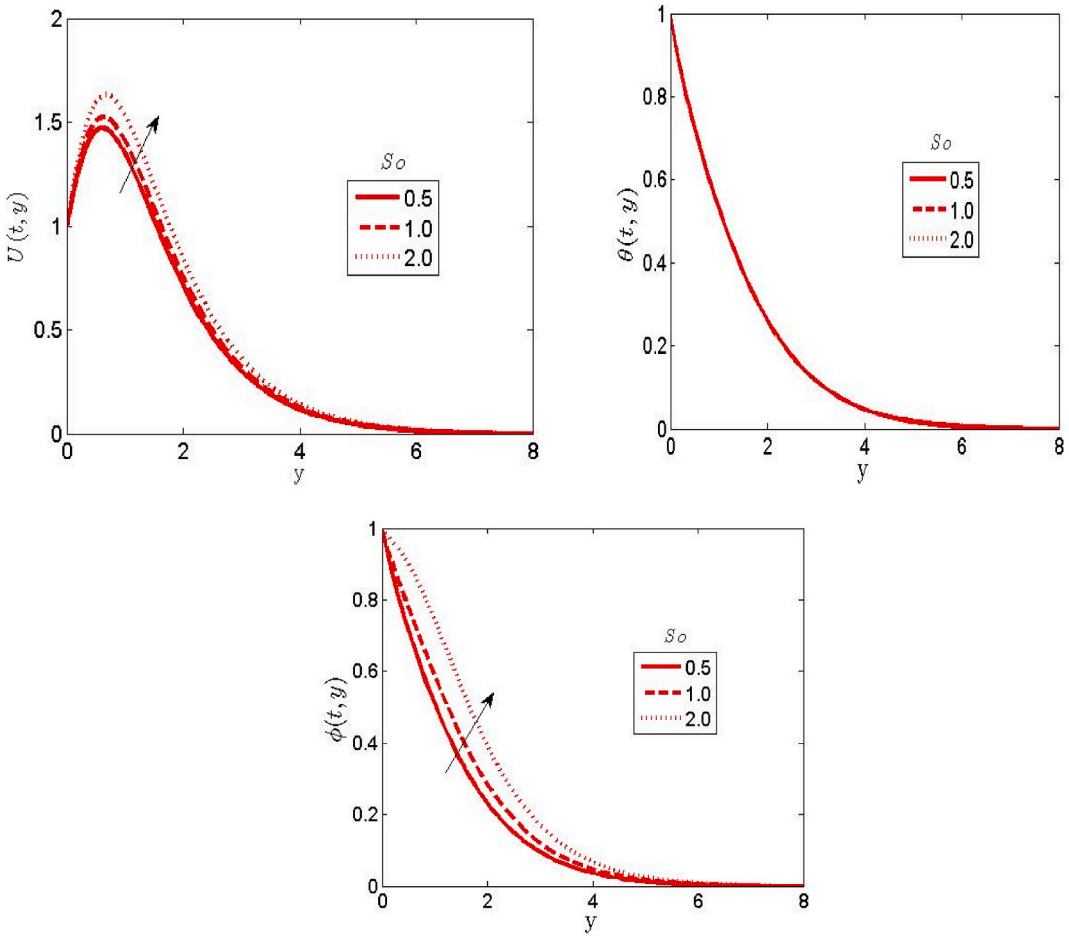

Fig. 3. Effect of Soret term on the velocity, temperature and concentration plots.

$$u = 1, \theta = 1 + \varepsilon e^{nt}, \varphi = 1 + \varepsilon e^{nt}, at \ \ y = 0 \tag{20}$$

$$u \to 0, \theta \to 0, \varphi \to 0, as \ \ y \to \infty \tag{21}$$

where $We, Gm, Ec, Sc, M, R, Du, Kr, Gr, Pr, \delta_x$ and So are Weissenberg number, mass Grahof number, Eckert number, Schmidt number, magnetic term, thermal radiation parameter, Dufour term, chemical reaction parameter, thermal Grashof number, Prandtl number, heat generation parameter and Soret term. The engineering quantities of curiosity are defined as follows:

Skin friction $(C_f) = \frac{\tau_w}{\rho v_0 u_0}$.

Nusselt number $(Nu) = \frac{-kq_w}{(T_w - T_\infty)}$.

Sherwood number $(Sh) = \frac{-Dq_m}{(C_w - C_\infty)}$.

1.2. Spectral relaxation technique

The transformed PDEs are solved numerically utilizing SRM. SRM is an iterative approach which uses the relaxation approach of Gauss-seidel type to decouple and linearize the coupled equations. The linearized equations will be discretize further and solved by employing the Chebyshev pseudo-spectral method. All linear terms in the level of iteration will be simplified at the current iteration noted as $r + 1$ while nonlinear terms is assumed known from the previous iteration noted as r. The basic steps of the spectral approach are:

(i) first decouple the nonlinear equations and linearize using Gauss-siedel techniques;
(ii) the linearized equations are further discretize; and
(iii) the discretized equations are solved iteratively by utilizing chebyshev pseudo-spectral technique.

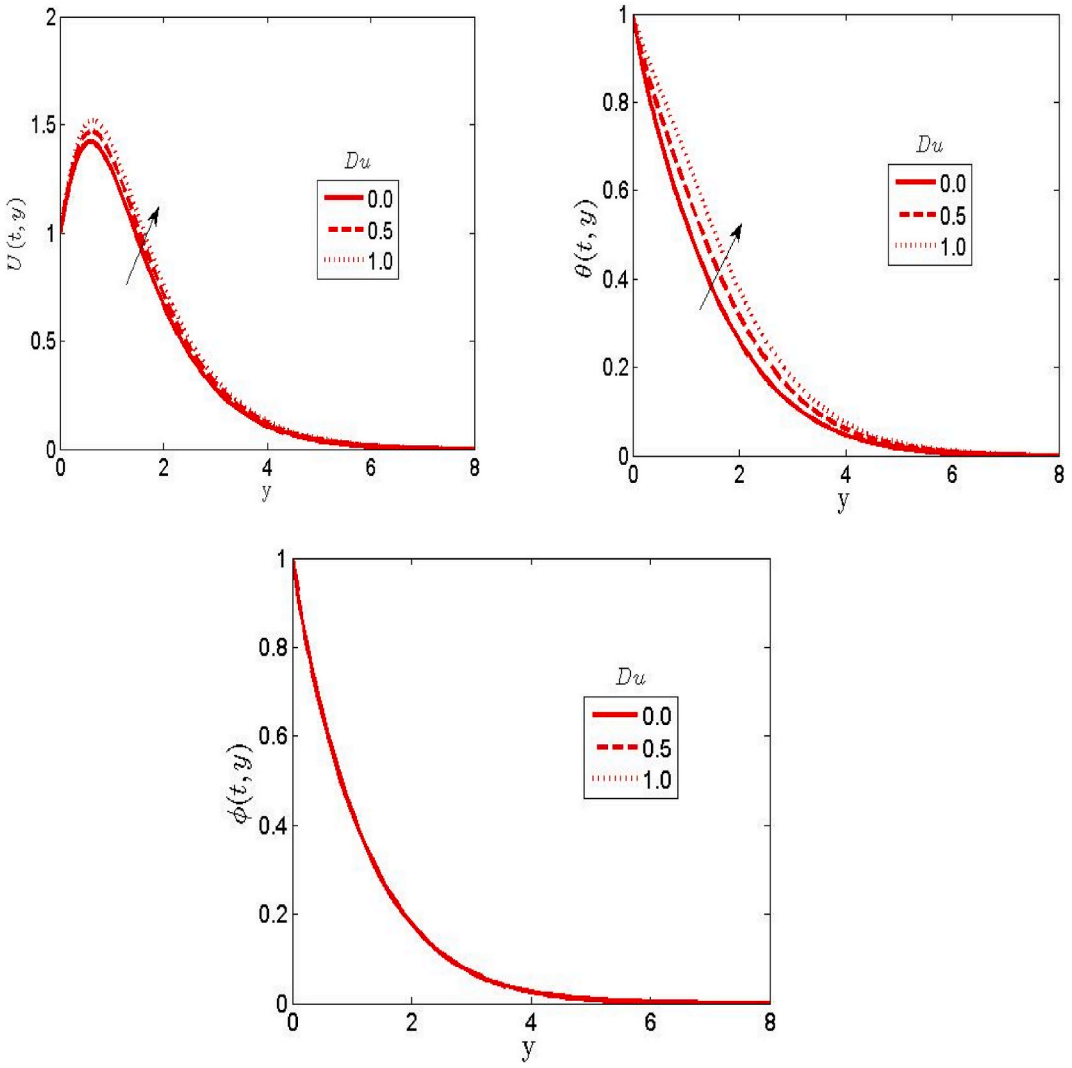

Fig. 4. Effect of Dufour term on velocity, temperature and concentration plots.

using the SRM on the non-linear couple PDEs (12)–(14) leads to:

$$\frac{\partial u_{r+1}}{\partial t} = (1+\varepsilon A e^{nt})\frac{\partial u_{r+1}}{\partial y} + (1-n)\frac{\partial^2 u_{r+1}}{\partial y^2} + nWe\frac{\partial u_{r+1}}{\partial y}\frac{\partial^2 u_{r+1}}{\partial y^2} - M^2 u_{r+1} + Gr\theta_r + Gm\varphi_r \tag{22}$$

$$\frac{\partial \theta_{r+1}}{\partial t} = (1+\varepsilon A e^{nt})\frac{\partial \theta_{r+1}}{\partial y} + \left(\frac{1+R}{Pr}\right)\frac{\partial^2 \theta_{r+1}}{\partial y^2} + Ec\left(\frac{\partial u_{r+1}}{\partial y}\right)^2 + Du\frac{\partial^2 \varphi_r}{\partial y^2} + \delta_s\theta_{r=1} + M^2 Ecu_{r+1}^2 \tag{23}$$

$$Sc\frac{\partial \varphi_{r+1}}{\partial t} = \frac{\partial^2 \varphi_{r+1}}{\partial y^2} + Sc\beta\frac{\partial \varphi_{r+1}}{\partial y} - Sck_r^2\varphi_{r+1} + ScSr\frac{\partial^2 \vartheta_{r+1}}{\partial y^2} \tag{24}$$

subject to

$$u_{r+1}(0,t) = 1, \vartheta_{r+1}(0,t) = 1 + \varepsilon e^{nt}, \varphi_{r+1}(0,t) = 1 + \varepsilon e^{nt} \tag{25}$$

$$u_{r+1}(\infty,t) = 0, \vartheta_{r+1}(\infty,t) = 0, \varphi_{r+1}(\infty,t) = 0 \tag{26}$$

defining coefficient parameters from above equations as:

$$\gamma = (1+\varepsilon A e^{nt}), \gamma_{0,r} = nWe\frac{\partial u_{n+1}}{\partial y}, \gamma_{1,r} = Gr\theta_r + Gm\varphi_r, \gamma_{2,r} = \left(\frac{1+R}{Pr}\right),$$

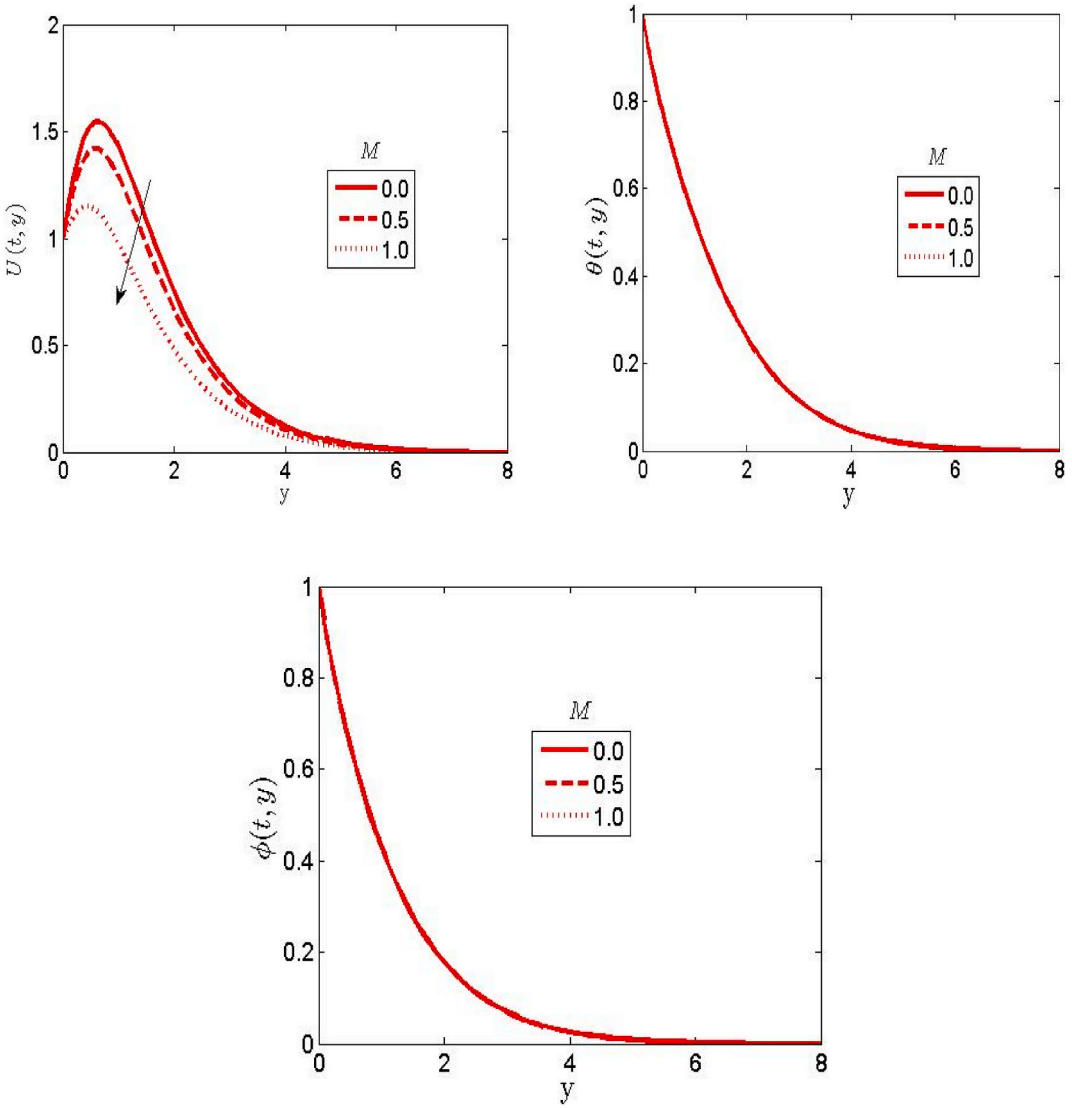

Fig. 5. Effect of magnetic parameter on the velocity, temperature and concentration plots.

$$\gamma_{3,r}=Ec\left(\frac{\partial u_{r+1}}{\partial y}\right)^2,\gamma_{4,r}=Du\frac{\partial^2\varphi_r}{\partial y^2},\gamma_{5,r}=M^2Ecu_{r+1}^2,\gamma_{6,r}=So\frac{\partial^2\theta_{r+1}}{\partial y^2} \tag{27}$$

putting the coefficient parameters above into (17)–(19) to obtain

$$\frac{\partial u_{r+1}}{\partial t}=\gamma\frac{\partial u_{r+1}}{\partial y}+(1-n)\frac{\partial^2 u_{r+1}}{\partial y^2}+\gamma_{0,r}\frac{\partial^2 u_{r+1}}{\partial y^2}-M^2u_{r+1}+\gamma_{1,r} \tag{28}$$

$$\frac{\partial\theta_{r+1}}{\partial t}=\gamma\frac{\partial\theta_{r+1}}{\partial y}+\gamma_{2,r}\frac{\partial^2\theta_{r+1}}{\partial y^2}+\gamma_{3,r}+\gamma_{4,r}+\delta_x\theta_{r+1}+\gamma_{5,r} \tag{29}$$

$$\frac{\partial\varphi_{r+1}}{\partial t}=\gamma\frac{\partial\varphi_{r+1}}{\partial y}+\frac{1}{Sc}\frac{\partial^2\varphi_{r+1}}{\partial y^2}-Kr\varphi_{r+1}+\gamma_{6,r} \tag{30}$$

subject to

$$u_{r+1}(0,t)=1,\vartheta_{r+1}(0,t)=1+\varepsilon e^{nt},\varphi_{r+1}(0,t)=1+\varepsilon e^{nt}\ \text{ at }\ y=0 \tag{31}$$

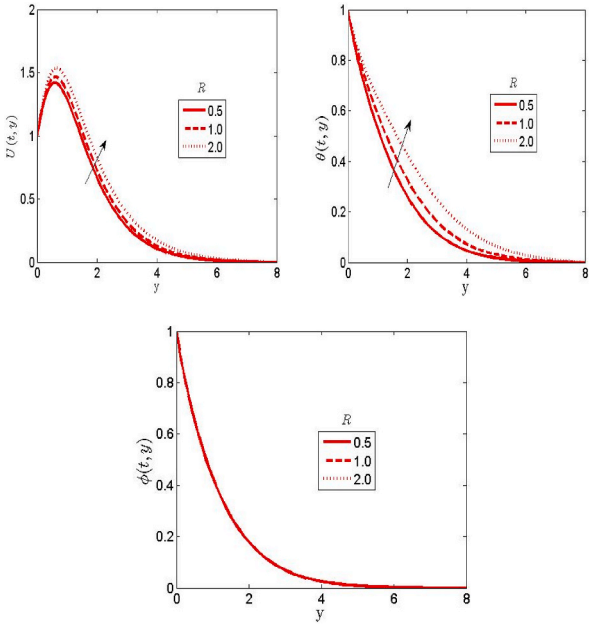

Fig. 6. Effect of thermal radiation term on the velocity, temperature and concentration plots.

$$u_{r+1}(\infty,t)=0,\theta_{r+1}(\infty,t)=0,\varphi_{r+1}(\infty,t)=0,\text{at } y\to\infty \tag{32}$$

The Gauss-Lobatto points given as follows is used to define the unknown functions

$$\xi_j=cos\frac{\pi j}{N},j=0,1,2,...,N;\ \ 1\le\xi\le-1 \tag{33}$$

here N signifies collocation points number. The physical region domain $[0,\infty]$ is simplified into $[-1,1]$. Thus, the problem is solved on $[0,L]$ and not $[0,\infty)$. The transformation defined below is used to map the interval

$$\frac{\eta}{L}=\frac{\xi+1}{2},-1\le\xi\le1 \tag{34}$$

here L signifies scaling term utilized in simplifying the boundary constraint at infinity. The initial simplification for solving equations 23–25 are gotten at $y=0$ and are considered subject to the boundary constraints (20) and (21). Hence, $u_0(y,t),\theta_0(y,t)$ and $\varphi_0(y,t)$ are chosen as;

$$u_0(y,t)=e^{-y},\theta_0(y,t)=\varphi_0(y,t)=e^{-y}+\varepsilon e^{nt} \tag{35}$$

The systematic equations 28–30 would be solved using iterative technique for unknown functions right from the initial approximations in (35). Schemes (28), (29), and (30) are iteratively solved for $u_{r+1}(y,t),\theta_{r+1}(y,t)$ and $\varphi_{r+1}(y,t)$ as $r=0,1,2$. In equations 28–30, we discretized by utilizing Chebyshev spectral collocation approach in the direction of y while implicit finite difference technique is utilized in the direction of t. The finite difference scheme is employed at mid-point between t^{n+1} and t^n. The mid-point is given as

$$t^{n+\frac{1}{2}}=\frac{t^{n+1}+t^n}{2} \tag{36}$$

Thus utilizing the centering about $t^{n+\frac{1}{2}}$ to the functions, say $u(y,t),\theta(y,t)$ and $\varphi(y,t)$ alongside associated derivative to obtain:

$$u\left(y_j,t^{n+\frac{1}{2}}\right)=u_j^{n+\frac{1}{2}}=\frac{u_j^{n+1}+u_j^n}{2},\left(\frac{\partial u}{\partial t}\right)^{n+\frac{1}{2}}=\frac{u_j^{n+1}-u_j^n}{\Delta t} \tag{37}$$

$$\theta\left(y_j,t^{n+\frac{1}{2}}\right)=\theta_j^{n+\frac{1}{2}}=\frac{\theta_j^{n+1}+\theta_j^n}{2},\left(\frac{\partial\theta}{\partial t}\right)^{n+\frac{1}{2}}=\frac{\theta_j^{n+1}-\theta_j^n}{\Delta t} \tag{38}$$

$$\varphi\left(y_j,t^{n+\frac{1}{2}}\right)=\varphi_j^{n+\frac{1}{2}}=\frac{\varphi_j^{n+1}+\varphi_j^n}{2},\left(\frac{\partial\varphi}{\partial t}\right)^{n+\frac{1}{2}}=\frac{\varphi_j^{n+1}-\varphi_j^n}{\Delta t} \tag{39}$$

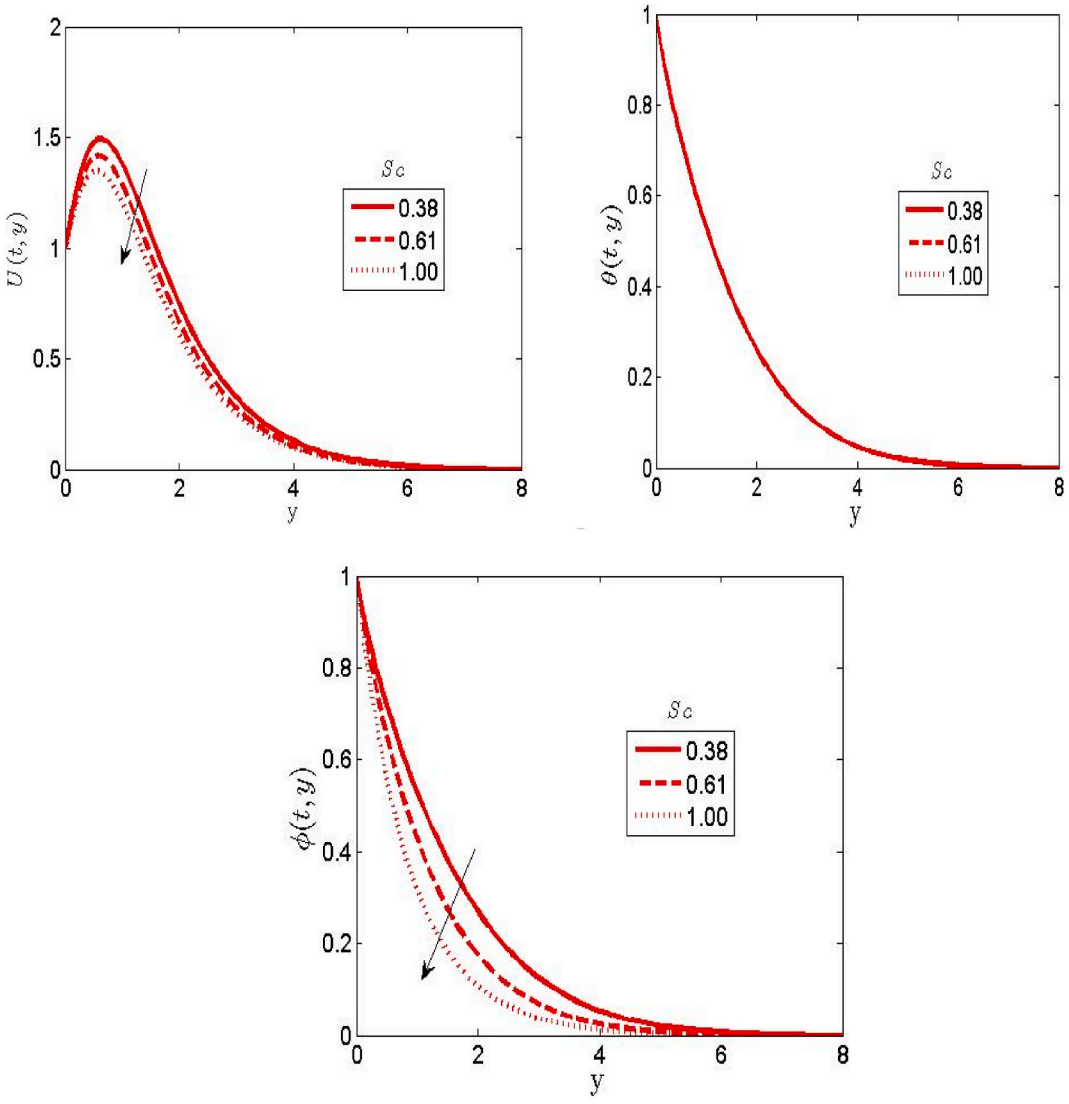

Fig. 7. Effect of Schmidt number on the velocity, temperature and concentration plots.

The spectral collocation approach requires the implementation of differentiation matrix D to evaluate the derivatives of variables unknown given as

$$\frac{d^r u}{dy^r} = \sum_{k=0}^{N} D_{ik}^r u(\xi_k) = D^r u, i = 0, 1, ...N \tag{40}$$

$$\frac{d^r \theta}{dy^r} = \sum_{k=0}^{N} D_{ik}^r \theta(\xi_k) = D^r \theta, i = 0, 1, ...N \tag{41}$$

$$\frac{d^r \varphi}{dy^r} = \sum_{k=0}^{N} D_{ik}^r \varphi(\xi_k) = D^r \varphi, i = 0, 1, ...N \tag{42}$$

The Chebyshev spectral collocation approach is first used on (28)-(30) followed by the finite differences.

$$\frac{du_{r+1}}{dt} = \left[\gamma D + (1-n)D^2 + \gamma_{0,r} D^2 - M^2\right] u_{r+1} + \gamma_{1,r} \tag{43}$$

$$\frac{d\theta_{r+1}}{dt} = \left[\gamma D + \gamma_{2,r} D^2 + \delta_x\right] \theta_{r+1} + \gamma_{3,r} + \gamma_{4,r} + \gamma_{5,r} \tag{44}$$

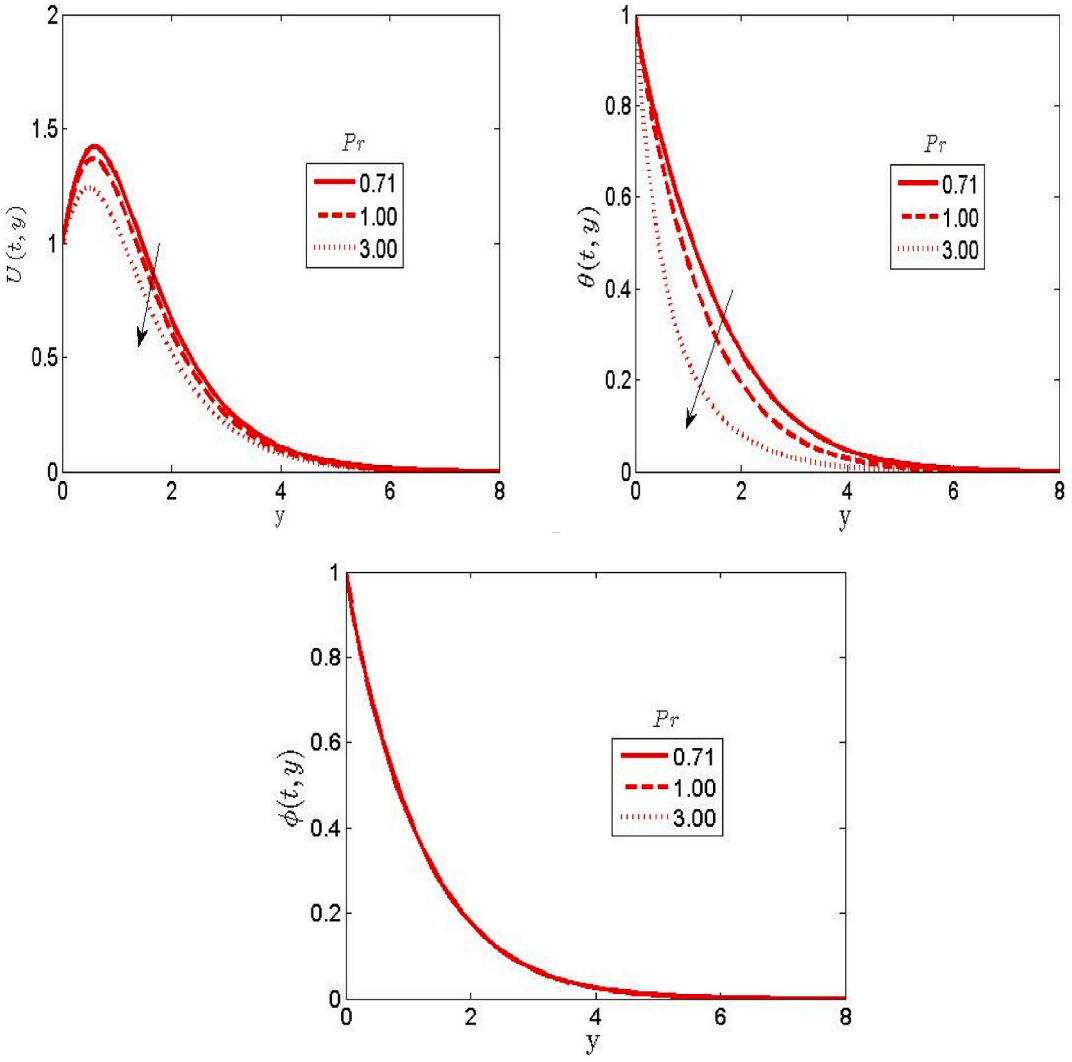

Fig. 8. Effect of Prandtl number on velocity, temperature and concentration plots.

$$\frac{d\varphi_{r+1}}{dt} = \left[\gamma D + \frac{1}{Sc}D^2 - Kr\right]\varphi_{r+1} + \gamma_{6,r} \tag{45}$$

subject to (20) and (21) where

$$u_{r+1} = \begin{bmatrix} u_{r+1}(x_0,t) \\ u_{r+1}(x_1,t) \\ \vdots \\ u_{r+1}(x_{N_{x-1}},t) \\ u_{r+1}(x_{N_x},t) \end{bmatrix}, \gamma_{0,r} = \begin{bmatrix} \gamma_{0,r}(x_0,t) & & & & \\ & \gamma_{0,r}(x_1,t) & & & \\ & & \ddots & & \\ & & & \ddots & \\ & & & & \gamma_{0,r}(x_{N_x},t) \end{bmatrix} \tag{46}$$

$$\theta_{r+1} = \begin{bmatrix} \theta_{r+1}(x_0,t) \\ \theta_{r+1}(x_1,t) \\ \vdots \\ \theta_{r+1}(x_{N_{x-1}},t) \\ \theta_{r+1}(x_{N_x},t) \end{bmatrix}, phi_{r+1} = \begin{bmatrix} \varphi_{r+1}(x_0,t) \\ \varphi_{r+1}(x_1,t) \\ \vdots \\ \varphi_{r+1}(x_{N_{x-1}},t) \\ \varphi_{r+1}(x_{N_x},t) \end{bmatrix} \tag{47}$$

From equation 40–42, the following scheme is obtained

$$M_1 u_{r+1}^{n+1} = M_2 u_{r+1}^{n} + K_1 \tag{48}$$

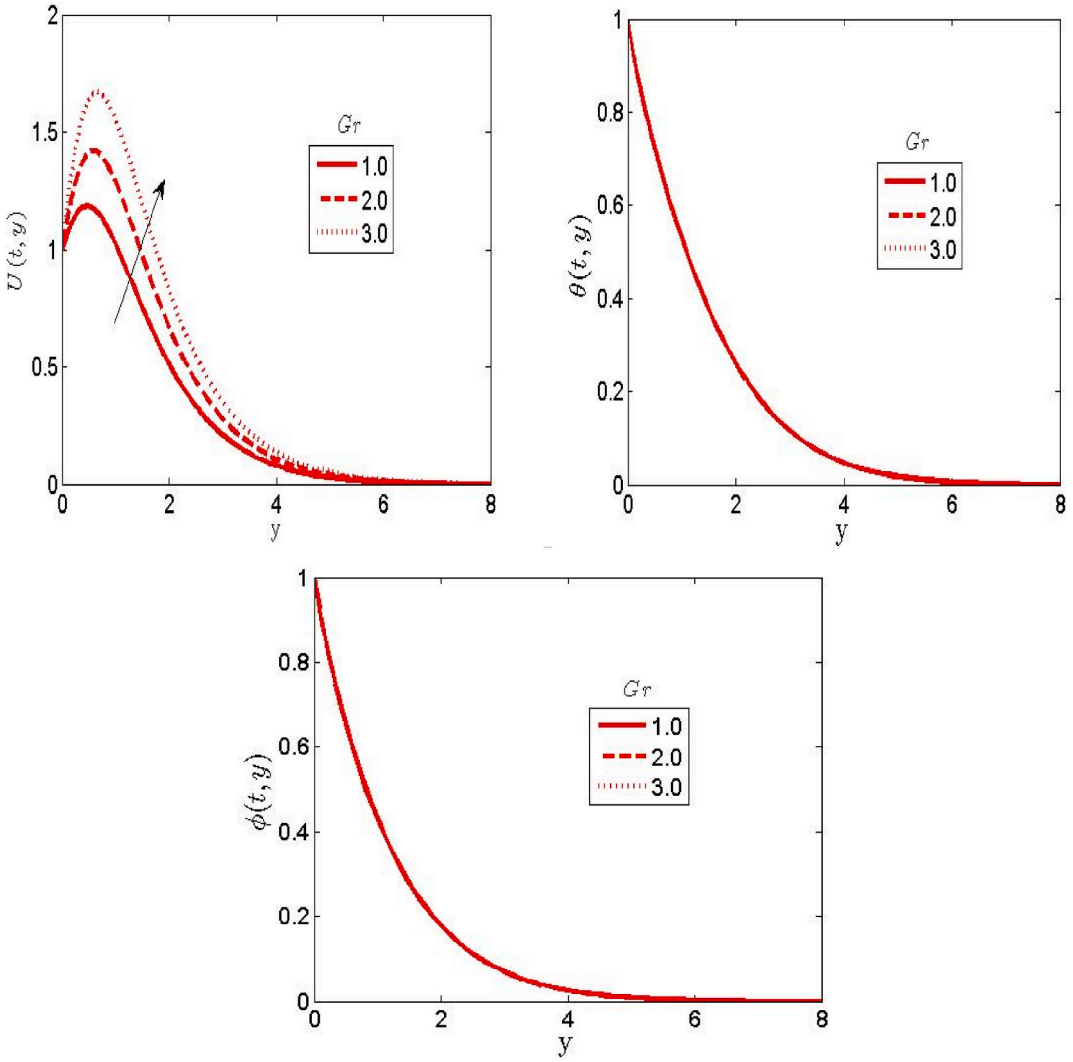

Fig. 9. Effect of thermal Grashof number on the velocity, temperature and concentration plots.

$$M_3\theta_{r+1}^{n+1} = M_4\theta_{r+1}^{n} + K_2 \tag{49}$$

$$M_5\varphi_{r+1}^{n+1} = M_6\varphi_{r+1}^{n} + K_3 \tag{50}$$

subject to the following initial and boundary conditions:

$$u_{r+1}(xN_x, t^n) = \theta_{r+1}(xN_x, t^n) = \varphi_{r+1}(xN_x, t^n) = 0 \tag{51}$$

$$u_{r+1}(x_0, t^n) = 1, \theta_{r+1}(x_0, t^n) = \varphi_{r+1}(x_0, t^n) = 1 + \varepsilon e^{nt}, n = 1, 2, \ldots \tag{52}$$

$$u_{r+1}(y_j, 0) = e^{-y_j}, \theta_{r+1}(y_j, 0) = \varphi_{r+1}(y_j, 0) = e^{-y_j} + \varepsilon e^{nt} \tag{53}$$

The above matrices are defined as;

$$M_1 = \frac{1}{2} - \frac{(\gamma D + (1-n)D^2 + \gamma_{0,r}D^2 - M^2)}{2}, M_2 = \frac{1}{2} + \frac{(\gamma D + (1-n)D^2 + \gamma_{0,r}D^2 - M^2)}{2}$$

$$M_3 = \frac{1}{2} - \frac{(\gamma D + \gamma_{2,r}D^2 + \delta_x)}{2}, M_4 = \frac{1}{2} + \frac{(\gamma D + \gamma_{2,r}D^2 + \delta_x)}{2}$$

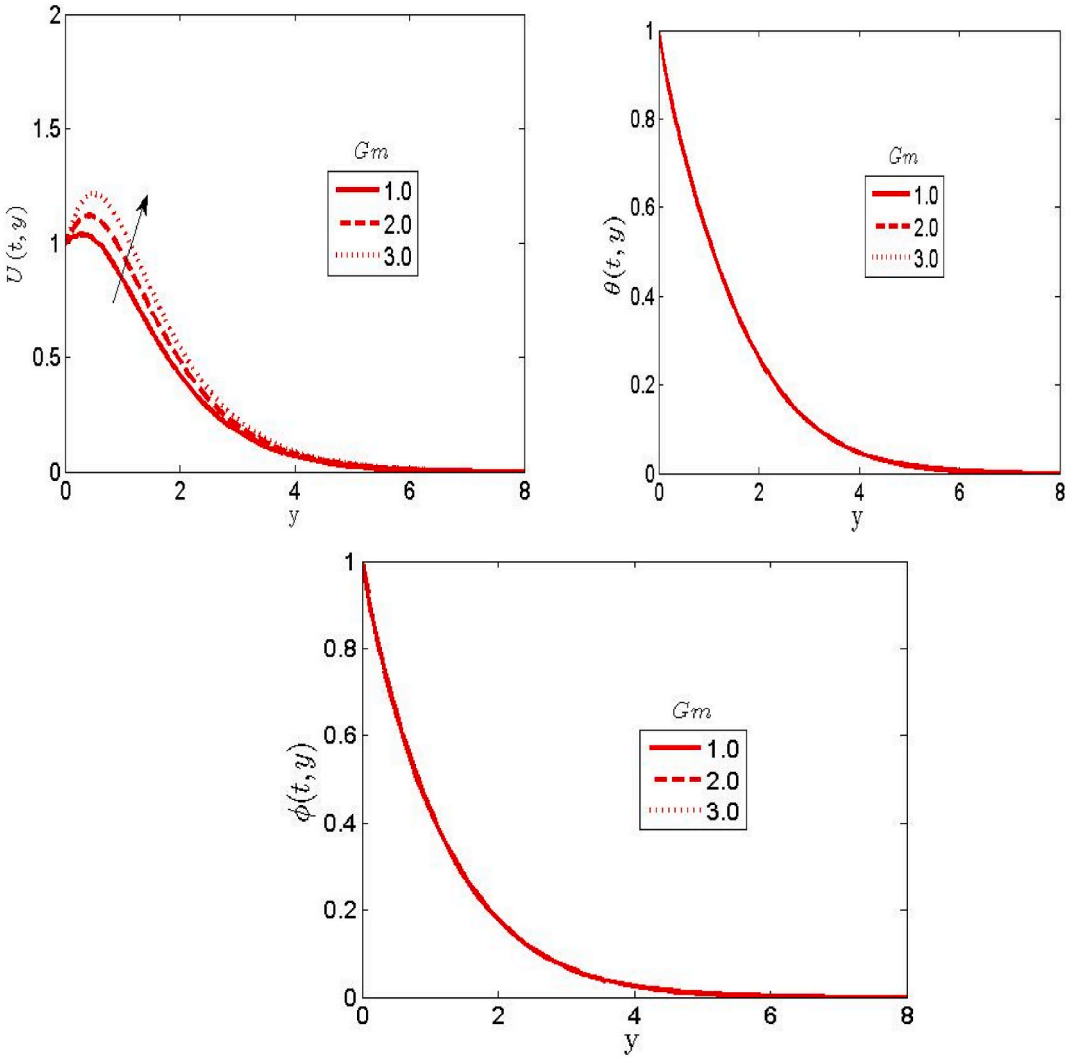

Fig. 10. Effect of mass Grashof number on the velocity, temperature and concentration plots.

$$M_5 = \frac{1}{2} - \frac{\gamma D + \frac{1}{Sc}D^2 - Kr}{2}, M_6 = \frac{1}{2} + \frac{\gamma D + \frac{1}{Sc}D^2 - Kr}{2}$$

2. Results and discussions

The equations that govern the fluid model are solved numerically via SRM. The effects of physical flow parameters on dimensionless concentration, velocity and temperature are presented in graphs and table. The default values of parameters are set to be We = M = 1,So = 0.6,Du = 0.9,R = 0.5,Sc = 0.61,Pr = 7.0,Gr = 2 Gm = 2,kr = 0.3 and Ec = 0.1.

Fig. 2 depicts the effect of Weissenberg number (We) on velocity, temperature and concentration respectively. It is noted in Fig. 2 that, an increase in We lowers the fluid motion by decelerating the velocity profile. The Weissenberg number is equivalent relaxation time. Therefore, a large values of We will bring enhancement to the relaxation time to allow greater resistance to the motion of the fluid by reducing the momentum layer thickness. The effect of We on temperature and concentration are found to be negligible with no effect on the profiles. The effect of the Soret term (So) on the temperature, velocity and concentration is depicted in Fig. 3. An increase in the values of So is observed to enhance the velocity alongside the concentration plot. This is owning to greater thermal diffusion as the values of So is raised. It worth noting that a positive Soret term leads to a stabilized effect. The moment So $>$ 0, a hike in temperature will lead to degeneration in density as well as mass fraction of specie concentration. It is refers to as cooperative solutal and thermal gradient as the solute spreads to coled regions. On the other hand, when So $<$ 0 a hike in temperature results to as competitive solutal and thermal gradient as the solute spreads to warmer regions. Hence, an elevation is noticed on the noticed on the velocity and concentration plot while the effect of So is negligible on the temperature plot. The outcomes in Fig. 3 is in good agreement with the outcome of [24].

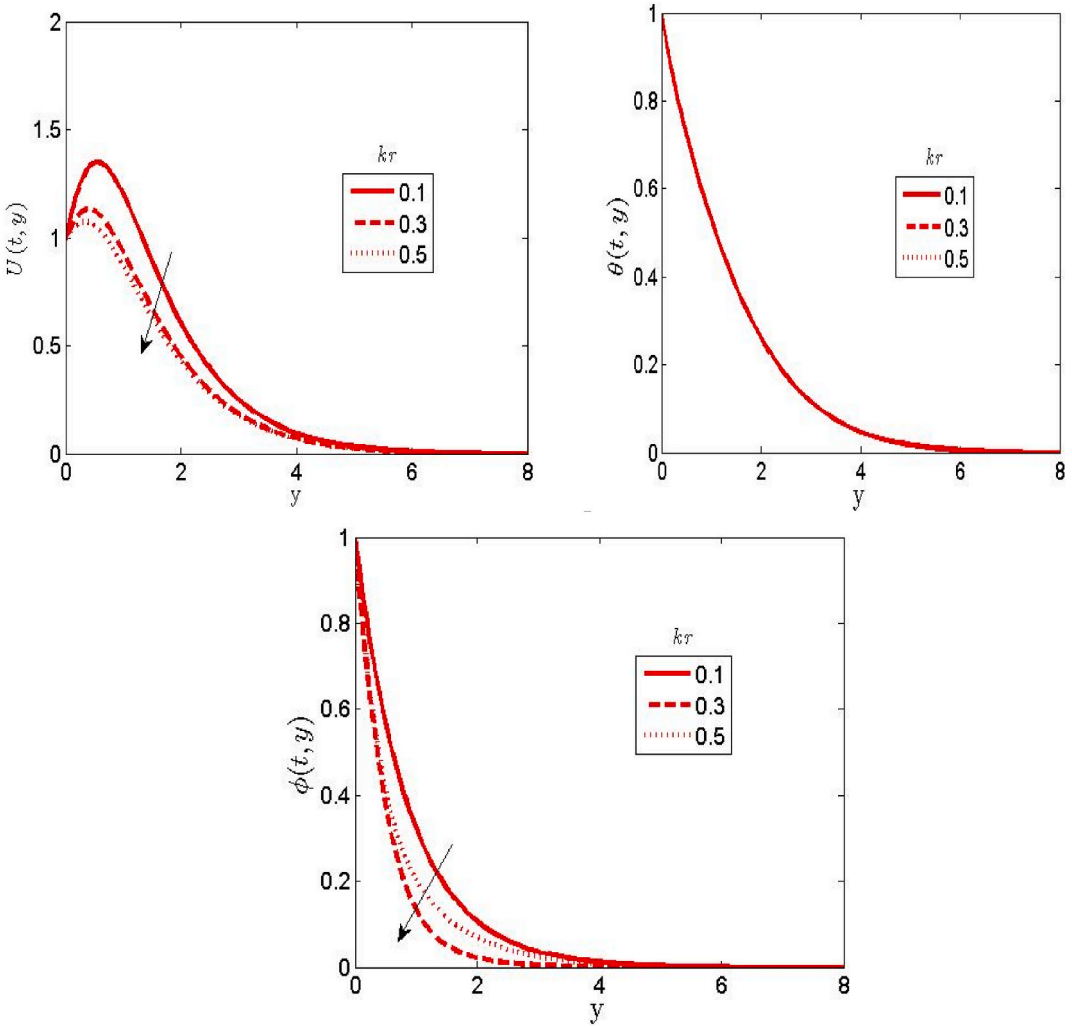

Fig. 11. Effect of chemical reaction term on the velocity, temperature and concentration plots.

The impact of Dufour term (Du) on the temperature, velocity and concentration plot is illustrated in Fig. 4. The Dufour term portrays the impact of concentration gradients on the temperature as noted in equation (8). It assist the flow and also have the tendency of boosting thermal energy within the layers. As depicted in Fig. 4, a large value of Du is detected to elevate the momentum as well as the thermal layer thickness. Hence, an increase in velocity and temperature plot is noticeable for a large value of Du. The effect of Du on concentration plot is negligible as shown in Fig. 4. Fig. 5 depicts the impact of the magnetic term (M) on the concentration, velocity and temperature plots. A degeneration in the velocity profile is noticeable for a large value of M while the effect of M is neglected on the temperature and concentration plots. This brings the existence of Lorentz force as the magnetic field is subjected in the direction of flow. This force acts not in favor of liquid velocity and thereby degenerate the velocity as well as the momentum layer thickness. Fig. 6 portrays the impact of the thermal radiation parameter (R) on the velocity, concentration and temperature plot. An increase in velocity and temperature is detected as the values of R increases. Physically, the thermal energy has great effect on the flow due to increase in R. As a result of this fact, the radiation has important on the flow when $R \neq 0$ and $R \to \infty$. Hence, an increase in the thermal condition, temperature and thermal layer is noticeable for a large value of R.

The effect of the Schmidt number (Sc) on velocity, temperature and concentration plot is depicted in Fig. 7. A large value of Sc causes both velocity and concentration plot to degenerate. Sc portrays the quotient of kinematic viscosity to fluid mass diffusivity; meaning $Sc = \nu/D$. Practically, $\nu > D$ signifies higher Sc and vice versa. The rate of mass transport degenerates owning to the effects of concentration buoyancy and lead to decrease in concentration plot. Hence, the outcomes in Fig. 7 shows higher viscosity compared to mass diffusivity. A large value of Sc shows no impact on the temperature plot. Fig. 8 illustrate the impact of the Prandtl number (Pr) on the velocity, temperature and concentration plot. An increase in Pr is noticed to degenerate the velocity and temperature plot. The Prandtl number explains the relationship with kinematic viscosity and thermal conductivity. Pr is very useful in coordinating the

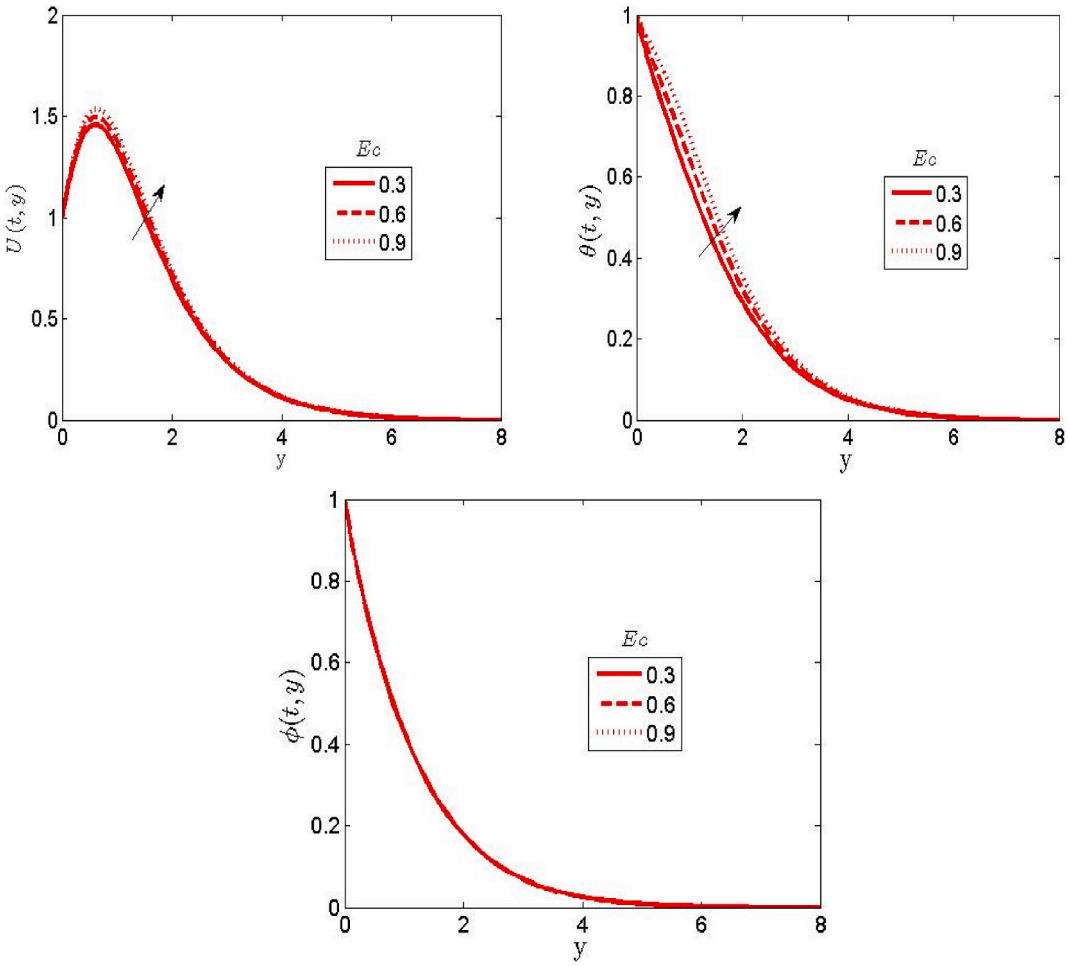

Fig. 12. Effect of Eckert number on the velocity, temperature and concentration plots.

Table 1
Numerical values for skin friction coefficient (C_f), Nusselt number (Nu), and sherwood number (Sh) for different values of We, M, Gr, Gm, R, Pr and Ec.

We	*M*	*Gr*	*Gm*	*R*	*Pr*	*Ec*	Cf	Nh	Sh
0.1							0.8242	0.6935	0.8633
0.3							1.7939	0.6935	0.8633
0.5							1.8345	0.6935	0.8633
	0.0						1.7682	0.5829	0.6335
	0.5						1.4328	0.5829	0.6335
	1.0						0.6530	0.5829	0.6335
		1.0					0.7499	0.6935	0.8100
		2.0					1.4328	0.6935	0.8100
		3.0					2.1156	0.6935	0.8100
			1.0				0.2285	0.6812	0.5179
			2.0				0.5296	0.6812	0.5179
			3.0				0.8306	0.6812	0.5179
				0.5			1.4228	0.6282	0.8335
				1.0			1.5399	0.6299	0.8335
				2.0			1.6906	0.7459	0.8335
					0.71		1.4328	0.6935	0.8633
					1.00		1.3073	0.8038	0.8633
					3.00		0.9461	1.5919	0.8633
						0.3	1.5316	0.5651	0.7968
						0.6	1.6306	0.4365	0.7968
						0.9	1.7295	0.3079	0.7968

Table 2
Numerical values for skin friction coefficient (C_f), Nusselt number (Nu), and sherwood number (Sh) for different values of Du, Sc, kr, So and δ_x.

Du	δ_x	Sc	kr	So	Cf	Nh	Sh
0.2					1.4028	0.8299	0.5179
0.4					1.5532	0.5559	0.5179
0.6					1.6736	0.4183	0.5179
	1.0				0.2051	2.4531	0.4121
	2.0				0.5934	3.1412	0.4121
	3.0				1.0241	3.5617	0.4121
		0.5			1.6072	0.3582	0.7169
		1.0			1.4265	0.3582	0.8701
		2.0			1.2463	0.3582	1.1372
			0.1		1.2533	0.9918	1.0904
			0.3		0.6173	0.9918	1.6939
			0.5		0.3992	0.9918	1.7030
				0.0	1.5606	0.9358	0.6993
				0.5	1.6885	0.9358	0.5353
				1.0	1.9443	0.9358	0.2074

thickening of momentum alongside thermal layers in heat transport analysis. Physically, any fluid with higher Pr possesses much viscosity which helps to lessens the hydrodynamics and thermal layer thickness by reducing the velocity and temperature plot. Thus, Pr is a good parameter for increasing the liquid flow rate of cooling. However, if $\Pr < 1$ the liquid is highly conducive. The effect of Pr on concentration is detected to be negligible.

Fig. 9 illustrate the impact of thermal Grashof number (Gr) on concentration, temperature and velocity plots. An upward increment in the velocity plot is detected as the value of Gr increases. In view of this, the thermal Grashof number acted like a buoyancy force on the fluid velocity alongside the hydrodynamic layer thickness. Buoyancy force portrays the upward liquid force exerted on the liquids. Experimentally, pressure hike the depth. Furthermore, the bottom pressure of the displaced object becomes very much than the force posses at the top. This implies that a net vertical force which elevate the velocity along with entire hydrodynamic layer thickness. The effect of Gr on temperature and concentration is negligible as shown in Fig. 9. The impact of the mass Grashof number (Gm) on the velocity, concentration and temperature plots is illustrated in Fig. 10. A large value of Gm is detected to hike the velocity plot and negligible on the temperature as well as concentration plot. This indicate that the mass Grashof number behaves like a mass buoyancy effect. In Fig. 11, an incremental value of chemical reaction parameter (kr) is discovered to degenerate the velocity alongside the concentration plot. Practically, the chemical reaction term alters the specie concentration by degenerating the solutal layer thickness. This indicate a destructive reaction on the fluids flow regime. The impact of Eckert number (Ec) is detected to elevate the velocity alongside the temperature plot in Fig. 12. Physically, the Eckert number is derived from the viscous dissipation added to the energy equation (8). Eckert number portrays the relationship between the enthapy in the flow and its kinetic energy. A high values of Ec elevate the shear forces in the liquids. Experimentally, heat energy is stored in the fluids owning to frictional heating and brings elevation to the thermal and hydrodynamic layer.

Table 1 shows the computational values for skin friction coefficient (C_f), Nusselt number (Nu) and Sherwood number (Sh) for encountered flow parameters. Increase in We is found to enhance the local skin friction and negligible on Sherwood and Nusselt number. A higher values of M is detected to degenerate the local skin friction. An incremental values of Gr and Gm is detected to hike the skin friction and negligible on the Nusselt and Sherwood number. An increase in R enhances the hydrodynamic and thermal layer thickness by enhancing skin friction and Nusselt number. A higher value of Pr is found to lessens the skin friction and elevate the Nusselt number. On the other hand, a higher value of Ec is found to hike the skin friction and lessens the Nusselt number. An increase in the values of Du and So is found to accelerate the skin friction while both effects are alternate on the Nusselt and Sherwood number. An increase in the values of Sc and kr is found to decelerate the skin friction and elevate the Sherwood number. The skin friction and Nusselt number is noticed to grow drastically with an increase in the heat generation parameter (see Table 2).

3. Conclusion

Analysis of unsteady MHD tangent hyperbolic liquid flow past a semi-infinite upward plate with Joule heating and influences of Soret-Dufour, viscous dissipation and thermal radiation has been scrutinized numerically. The Rosseland diffusion model has been employed on the simplified coupled nonlinear PDEs to check the behaviour of radiative heat flux. The outcomes to the present analysis is gotten by utilizing SRM. SRM is expressed in term of Lagrange polynimials interpolation employed to decouple systems of PDEs by employing relaxation approach. The following final remarks are drawn from the outcomes:

(i) An incremental values of Weissenberg number is found to degenerate the velocity profile;
(ii) An increase in Soret term is found to elevate the velocity alongside the concentration profile;
(iii) The velocity alongside the temperature plot is found to increase as a result of increasing the Dufour term;
(iv) The transverse magnetism is found to increase the strength of the Lorentz force as the velocity profile degenerates; and
(v) The velocity alongside the concentration plot is found to degenerate owning to increase in the Schmidt number.

The outcomes of this study would be useful in drilling operations, polymer engineering and bioengineering. Owning to the MHD nature of the liquid, this outcomes is of interest in controlling magnetized metal welding and coating of metals. The outcomes of this study would also be useful in separating isotopes.

Declaration of competing interest

The authors declare that they have no conflict of interest.

References

[1] A. Hussain, M.Y. Malik, T. Salahuddin, A. Rubab, Mair Khan, Effects of viscous dissipation on MHD tangent hyperbolic fluid over a nonlinear stretching sheet with convective boundary conditions, Results Phys. 7 (2017) (2017) 3502–3509.

[2] N. Vijaya, Y. Hari Krishna, K. Kalyani, G.V.R. Reddy, Soret and radiation effects on an unsteady flow of a casson fluid through porous vertical channel with expansion and contraction, Front. Heat Mass Transf. 11 (2018).

[3] G.V.R. Reddy, Y.H. Krishna, Soret and dufour effects on MHD micropolar fluid flow over a linearly stretching sheet, through a non-Darcy porous medium, Int. J. Appl. Mech. Eng. 23 (2) (2018) 485–502.

[4] K. Suneetha, S.M. Ibrahim, G.V. Ramana Reddy, A study on free convective heat and mass transfer flow through a highly porous medium with radiation, chemical reaction and soret effects, J. Comput. Appl. Res. Mech. Eng. 8 (2) (2019) 121–132.

[5] N. Vijaya, P. Krishna Jyothi, A. Anupama, R. Leelavathi, K. Ambica, Thermophoresis and Buoyancy Effects on Chemically reactive upper convected maxwellnfluid induced by an exponentially stretching sheet: applications Cattaneo-Christov heat flux, Front. Heat Mass Transf. 17 (2021) 23, this link is disabled.

[6] W. Ibrahim, Magnetohydrodynamics (MHD) flow of a tangent hyperbolic fluid with nanoparticles past a stretching sheet with second order slip and convective boundary condition, Results Phys. 7 (2017) (2017) 3723–3731.

[7] Munagala Rao, Venkata Subba, Kotha Gangadhar, Giulio Lorenzini, A computational analysis for boundary layer flow of magneto hydrodynamic tangent hyperbolic fluid of heat and mass transfer past a stretching cylinder with suction/injection using spectral relaxation method, Math. Modell. Eng. Prob. 6 (No 1) (2019) 38–46.

[8] M. Naseer, Muhammad Yousaf Malik, Sohail Nadeem, Abdul Rehman, The boundary layer flow of hyperbolic tangent fluid over a vertical exponentially stretching cylinder, Alex. Eng. J. 53 (2014) 747–750, 2014.

[9] GulZaman ZakirUllah, Lie group analysis of magnetohydrodynamic tangent hyperbolic fluid flow towards a stretching sheet with slip conditions, Heliyon 3 (2017), e00443, 10 .1016/j .heliyon .2017 .e00443.

[10] A. Mahdy, G.A. Hoshoudy, Two-phase mixed convection nanofluid flow of a dusty tangent hyperbolic past a nonlinearly stretching sheet, J. Egyp. Math. Soci. 27 (2019) 44, 2019.

[11] M. Ali Abbas, Y.Q. Bai, M.M. Bhatti, M.M. Rashidi, Three dimensional peristaltic flow of hyperbolic tangent fluid in non-uniform channel having flexible walls, Alex. Eng. J. 55 (2016) 653–662, 2016.

[12] F.I. Alao, A.I. Fagbade, B.O. Falodun, Effects of thermal radiation, Soret and Dufour on an unsteady heat and mass transfer flow of a chemically reacting fluid past a semi-infinite vertical plate with viscous dissipation, J. Nig. Math. Soci. 35 (2016) (2016) 142–158.

[13] P. Bala Anki Reddy, Magnetohydrodynamic flow of a Casson fluid over an exponentially inclined permeable stretching surface with thermal radiation and chemical reaction, Ain Shams Eng. J. 7 (2016) 593–602, 2016.

[14] Kh Hosseinzadeh, A. Jafarian Amiri, S. Saedi Ardahaie, D.D. Ganji, Effect of variable lorentz forces on nanofluid flow in movable parallel plates utilizing analytical method, Case Stud. Therm. Eng. 10 (2017) (2017) 595–610.

[15] S.S. Ghadikolaei, Kh Hosseinzadeh, D.D. Ganji, Analysis of unsteady MHD Eyring-Powell squeezing flow in stretching channel with considering thermal radiation and Joule heating effect using AGM, Case Stud. Therm. Eng. 10 (2017) (2017) 579–594.

[16] T. Hayat, Sajjad Rai, Taseer Muhammad, Alsaedi Ahmed, Rahmat Ellahi, On MHD nonlinear stretching flow of Powell–Eyring nanomaterial, Results Phys. 7 (2017) (2017) 535–543.

[17] Zahir Shah, Ebenezer Bonyah, Saeed Islam, Waris Khan, Mohammad Ishaq, Radiative MHD thin film flow of Williamson fluid over an unsteady permeable stretching sheet, Heliyon 4 (2018), e00825.

[18] A.S. Idowu, B.O. Falodun, Variable thermal conductivity and viscosity effects on non-Newtonian fluids flow through a vertical porous plate under Soret-Dufour influence, Math. Comput. Simulat. 177 (2020) (2020) 358–384.

[19] M.G. Sobamowo, Combined effects of thermal radiation and nanoparticles on free convection flow and heat transfer of casson fluid over a vertical plate, Int. J. Chem. Eng. 2018 (2018) 25, https://doi.org/10.1155/2018/7305973. Article ID 7305973.

[20] K. Jabeen, M. Mushtaq, R.M. Akram Muntazir, Analysis of MHD fluids around a linearly stretching sheet in porous media with thermophoresis, radiation, and chemical reaction, Math. Probl Eng. 2020 (2020), https://doi.org/10.1155/2020/9685482. Article ID 9685482, 14 pages.

[21] K. Ganesh Kumar, B.J. Gireesha, R.S.R. Gorla, Flow and heat transfer of dusty hyperbolic tangent fluid over a stretching sheet in the presence of thermal radiation and magnetic field, Int. J. Mech. Mater. Eng. 13 (2018) (2018) 2, https://doi.org/10.1186/s40712-018-0088-8.

[22] A.I. Fagbade, B.O. Falodun, A.J. Omowaye, MHD natural convection flow of viscoelastic fluid over an accelerating permeable surface with thermal radiation and heat source or sink: spectral Homotopy Analysis Approach, Ain Shams Eng. J. 9 (2018) 1029–1041, 2018.

[23] F.D. Ayegbusi, Cletus Onwubuoya, Bidemi O. Falodun, Unsteady problem of magneto hydrodynamic heat plus mass transfer convective flow over a moveable plate with effects of thermophoresis and thermal radiation, Heat Trans. 49 (2020) (2020) 3593–3612.

[24] A.S. Idowu, B.O. Falodun, Soret–Dufour effects on MHD heat and mass transfer of Walter's-B viscoelastic fluid over a semi-infinite vertical plate: spectral relaxation analysis, J. Taibah Univ. Sci. 13 (1) (2019) 49–62, https://doi.org/10.1080/16583655.2018.1523527.

[25] Y. Damodhar Reddy, Fateh Mebarek-Oudina. Radiation, velocity and thermal slips effect toward MHD boundary layer flow through heat and mass transport of Williamson nanofluid with porous medium, 2022. DOI: 10.1007/s13369-022-06825-2.

[26] Marzougui. Souad, Mebarek-Oudina. Fateh, Magherbi. Mourad, Mchirgui Ali, Entropy generation and heat transport of Cu–water nanoliquid in porous lid-driven cavity through magnetic field 32 (6) (2022) 2047–2069. https://doi.org/10.1108/HFF-04-2021-0288.